

CHALLENGING COSMIC RAY PROPAGATION WITH ANTIPROTONS. EVIDENCE FOR A “FRESH” NUCLEI COMPONENT?

IGOR V. MOSKALENKO¹

NASA/Goddard Space Flight Center, Code 661, Greenbelt, MD 20771

ANDREW W. STRONG

Max-Planck-Institut für extraterrestrische Physik, Postfach 1603, D-85740 Garching, Germany

STEPAN G. MASHNIK

Los Alamos National Laboratory, Los Alamos, NM 97545

AND

JONATHAN F. ORMES

NASA/Goddard Space Flight Center, Code 600, Greenbelt, MD 20771

ABSTRACT

Recent measurements of the cosmic ray (CR) antiproton flux have been shown to challenge existing CR propagation models. It was shown that the reacceleration models designed to match secondary to primary nuclei ratios (e.g., boron/carbon) produce too few antiprotons. Matching both the secondary to primary nuclei ratio and the antiproton flux requires artificial breaks in the diffusion coefficient and the primary injection spectrum suggesting the need for other approaches.

In the present paper we discuss one possibility to overcome these difficulties. Using the measured antiproton flux *and* B/C ratio to fix the diffusion coefficient, we show that the spectra of primary nuclei as measured in the heliosphere may contain a fresh local “unprocessed” component at low energies perhaps associated with the Local Bubble, thus decreasing the measured secondary to primary nuclei ratio. The independent evidence for SN activity in the solar vicinity in the last few Myr supports this idea. The model reproduces antiprotons, B/C ratio, and elemental abundances up to Ni ($Z \leq 28$). Calculated isotopic distributions of Be and B are in perfect agreement with CR data. The abundances of three “radioactive clock” isotopes in CR, ¹⁰Be, ²⁶Al, ³⁶Cl, are all consistent and indicate a halo size $z_h \sim 4$ kpc based on the most accurate data taken by the ACE spacecraft.

Subject headings: diffusion — elementary particles — nuclear reactions, nucleosynthesis, abundances — cosmic rays — ISM: general — Galaxy: general

1. INTRODUCTION

The spectrum and origin of antiprotons in CR has been a matter of active debate since the first reported detections in balloon flights (Golden et al. 1979; Bogomolov et al. 1979). Because of the baryonic asymmetry of the Universe, antiprotons are not found at rest. There is a consensus that most of the CR antiprotons observed near the Earth are “secondaries” produced in collisions of energetic CR particles with interstellar gas (e.g., Mitchell et al. 1996).

The spectrum of secondary antiprotons has a peak at about 2 GeV decreasing sharply towards lower energies. This unique shape distinguishes antiprotons from other cosmic-ray species and allows for searches of primary antiprotons at low energies. Over the last few years the accuracy has been improved sufficiently (BESS 1995–2000, Orito et al. 2000; Sanuki et al. 2000; Asaoka et al. 2002) that we can restrict the spectrum of the secondary component accurately enough to test Galactic CR propagation models, and the heliospheric modulation.

It has been recently shown (Moskalenko et al. 2002) that accurate antiproton measurements during the last solar minimum 1995–1997 (BESS, Orito et al. 2000) are inconsistent with existing propagation models at the $\sim 40\%$ level at about 2 GeV while the stated measurement uncertainties in this energy range are now $\sim 20\%$. The conventional models based on local CR measurements, simple energy dependence of the diffusion coefficient, and uniform CR source spectra throughout the Galaxy fail to reproduce simultaneously both the secondary to primary nuclei ratio and antiproton flux.

The reacceleration model designed to match secondary to primary nuclei ratios (e.g., boron/carbon) produce too few antiprotons because, e.g., matching the B/C ratio at all energies requires the diffusion coefficient to be too large. The models without reacceleration can reproduce the antiproton flux, however they fall short of explaining the low-energy decrease in the secondary to primary nuclei ratio. To be consistent with both, the introduction of breaks in the diffusion coefficient and the injection spectrum is required, which would suggest new phenomena in particle

¹Joint Center for Astrophysics, University of Maryland, Baltimore County, Baltimore, MD 21250

acceleration and propagation.

Recently there has appeared some indication that the atmospheric contribution to the antiproton flux measured in the upper atmosphere is underestimated. If this is true, the reacceleration model could still be the best one to describe propagation of nucleon species in the Galaxy (for more details see Section 8). However, in this work we have assumed the published Galactic antiproton flux, corrected for atmospheric production, is accurate.

In the present paper we discuss another possibility to overcome the difficulties encountered by reacceleration models. We will show that the inclusion of a local primary component at low energies, perhaps associated with the Local Bubble (LB), reconciles the data.

2. INTERSTELLAR COSMIC RAY SPECTRUM

Just as secondary nuclei, the product of the disintegration of primary nuclei, are abundant in CR but rare in the interstellar medium (ISM), diffuse γ -rays, antiprotons, and positrons are secondary products of interactions of mostly CR protons and helium nuclei with interstellar gas. The CR propagation model that describes any secondary to primary ratio should equally well describe all the others: B/C, sub-Fe/Fe, \bar{p}/p ratios, and spectra of nuclei, positrons, and diffuse Galactic continuum γ -rays.

The diffusive reacceleration models naturally reproduce secondary to primary nuclei ratios in CR and agree better with K-capture parent/daughter nuclei ratio (e.g., see Jones et al. 2001), though this result is not completely conclusive due to the large error bars in CR measurements and uncertainties in important isotopic cross sections. It is, however, clear that some reacceleration is unavoidable in the ISM. Because of the unique shape of the antiproton spectrum, reacceleration has much weaker effect on it than in the case of nuclei. Taking into account that the antiproton production spectrum can be calculated accurately, antiprotons provide a unique complementary tool to test propagation models (and heliospheric modulation).

Our previous result (Moskalenko et al. 2001b, 2002), in agreement with calculations of other authors (Molnar & Simon 2001), was that matching the secondary/primary nuclei ratio B/C using reacceleration models leads to values of the spatial diffusion coefficient apparently too large to produce the required antiproton flux, when the propagated nucleon spectra are tuned to match the local proton and helium flux measurements. This is an essential shortcoming.

Assuming the measured antiproton flux is correct and the current heliospheric modulation models are approximately right, we have the following possibility to reconcile the B/C ratio with the required flux of secondary antiprotons. The spectra of primary nuclei as measured in the heliosphere may contain a fresh local “unprocessed” component at low energies thus decreasing the measured secondary to primary nuclei ratio. This component would have to be local in the sense of being specific to the so-

lar neighbourhood, so that the well-known “Local Bubble” phenomenon is a natural candidate.

The idea that CR are accelerated out of SN ejecta-enriched matter in superbubbles has been discussed in numerous papers (e.g., Higdon, Lingenfelter, & Ramaty 1998, and references therein). The possibility that the “fresh” component is coming from the Local Bubble has been discussed by, e.g., Morfill & Freyberg (1998) and Davis et al. (2000). We will hereafter call it the “Local Bubble Hypothesis.” The idea is that primary CR like ^{12}C and ^{16}O have a local component at low energies, while secondary CR like B are produced Galaxy-wide over the confinement time of 10–100 Myr. Then the B/C ratio will be lower at low energies than expected in a uniform model, due to the enhanced local C (and the reduced Galactic production of B). If this idea is correct then the high-energy part of the secondary/primary nuclei ratio plus the measured antiproton flux at maximum, ~ 2 GeV, can be used to restrict the value and energy dependence of the diffusion coefficient, while the required contribution of the local sources can be derived from the measured secondary/primary nuclei ratio at low energies.

One additional hint for the possible existence of an “unprocessed” component is the calculated ratio of $^{13}\text{C}/^{12}\text{C} \sim 0.14$ at 120 MeV/nucleon (modulation potential 500 MV), which appears to be a factor of two larger than that observed when the propagation parameters are tuned to the B/C ratio (Moskalenko et al. 2002). The isotope ^{13}C is almost all secondary, as are Be and B isotopes. Since the primary source of ^{13}C is ^{16}O , accounting for as much as $\sim 60\%$ of the total, this may indicate an “over-enrichment” of the assumed source abundances in oxygen. If so, the “over-enrichment” may be true also for primary carbon, but tuning to the observed B/C artificially eliminates the excess of lithium, beryllium, and boron. We note that the ratio of $^{15}\text{N}/^{16}\text{O}$ is, however, correct, and the problem with overproduction of ^{13}C may arise from cross section errors ² (see Appendix A).

3. THE LOCAL BUBBLE HYPOTHESIS

The low-density region around the sun, filled with hot H I gas, is called the Local Bubble (e.g., Sfeir et al. 1999). The size of the region is about 200 pc, and it is likely that it was produced in a series of supernova (SN) explosions. Most probably its progenitor was an OB star association. Though people discuss different scenarios (e.g., Maíz-Apellániz 2001; Berghöfer & Breitschwerdt 2002), the LB age and the number of SN progenitors appears to be similar, ~ 10 Myr and $\sim 10 - 20$ SN, respectively. Most probably they exploded as core-collapse SN II or thermonuclear SN Ib/c with a mass of pre-SN stars between several and $\sim 10M_{\odot}$, with the last SN explosion occurring approximately 1–2 Myr ago, or 3 SN occurring within the last 5 Myr.

There is also some evidence of a SN explosion nearby. An excess of ^{60}Fe measured in a deep ocean core sam-

²The production cross sections of $^{14,15}\text{N}$, and $^{12,13}\text{C}$ have been measured only in a narrow energy range.

ple of ferromanganese crust suggests the deposition of SN-produced iron on earth (Knie et al. 1999). The enhanced concentrations were found in two of three layers corresponding to a time span of < 2.8 Myr and $3.7\text{--}5.9$ Myr, respectively. The study suggests a SN explosion about 5 Myr ago at 30 pc distance. Another study reports an enhancement in the CR intensity dated about 40 kyr ago (Sonett, Morfill, & Jokipii 1987), which is interpreted as the passage across the solar system of the shock wave from a SN exploding about 0.1 Myr ago. Taking into account possible errors of all these estimates, they point to a nearby SN explosion some 1 Myr ago (see also discussion in Benítez, Maíz-Apellániz, & Canelles 2002).

It could also be that “fresh” LB contributions from continuous acceleration in the form of shock waves (Bykov & Fleishman 1992), and/or energetic particles coming directly from SN remnants still influence the spectra and abundances of local CR. The elemental abundances of the low-energy nonthermal component in a superbubble can differ strongly from the standard cosmic abundances (Bykov 2001) due to ejection of matter enriched with heavy elements from SN and stellar winds of massive stars (Wolf-Rayet, OB stars). The continuous acceleration is connected with the lifetime of a shock wave in the LB. A reasonable estimate is given by the sound crossing time, approximately 2 Myr, for a distance of 200 pc in a 10^6 K plasma (Berghöfer & Breitschwerdt 2002). On the other hand, the particle crossing time can be estimated as $t \sim x^2/D \sim 1$ Myr for a typical value of the diffusion coefficient in the ISM $D \sim 10^{28}$ cm s $^{-2}$ and $x \sim 200$ pc. Therefore, accelerated particles are expected to be present in this region.

4. THE CALCULATION PROCEDURE

In our calculations we use the propagation model GALPROP³ as described elsewhere (Strong & Moskalenko 1998; Moskalenko et al. 2002); for the present purpose the 2D cylindrically symmetrical option is sufficient. For a given halo height z_h the diffusion coefficient as a function of momentum and the reacceleration or convection parameters is determined by data on secondary-to-primary ratios in CR. The spatial diffusion coefficient is taken as $D_{xx} = \beta D_0 (\rho/\rho_0)^\delta$; the corresponding diffusion in momentum space and other details of the models can be found in our earlier papers. We use our standard methodologies and include two types of cosmic ray sources.

Antiproton production and propagation are calculated as described in Moskalenko et al. (2002).

The nucleon injection spectrum of the Galactic component was taken as a modified power-law in rigidity (Jones et al. 2001), $dq(p)/d\rho \propto \rho^{-\gamma}/\sqrt{1 + (\rho/2)^{-2}}$, for the injected particle density. The proton and He spectra are tuned to the local measurements as described in Moskalenko et al. (2002).

The LB spectrum is taken to have the form (as suggested by Bykov & Fleishman 1992 and Bykov 2001 for continuous acceleration by interstellar shocks): $df/d\rho \propto$

$\rho^{-\eta} \exp(-\rho/\rho_b)$, where ρ is the rigidity, and ρ_b is the cut off rigidity. ρ_b and the LB source abundances are adjustable parameters. In terms of kinetic energy per nucleon E this can be re-written as

$$\frac{df}{dE} = a(Z, A) \frac{A(E+m)}{Zp} \rho^{-\eta} \exp(-\rho/\rho_b), \quad (1)$$

where $a(Z, A)$ is the abundance of a nucleus (Z, A) , Z, A are the nucleus charge and atomic number, correspondingly, m is the atomic mass unit, p is the momentum per nucleon, $\rho_b = \frac{A}{Z} \sqrt{(E_b + m)^2 - m^2}$. The particular spectral shape of the LB component is not important as long as it decreases sharply towards high energies and is much softer than the Galactic CR spectrum. We show the results obtained with $\eta = 1$, but they are very similar with $\eta = 2$ with ρ_b adjusted correspondingly.

The procedure to tune the CR elemental abundances, secondary/primary nuclei ratios, and antiproton flux we adopted was as follows. The high energy part of B/C ratio and antiproton flux measurements are used to restrict the value of the diffusion coefficient and its energy dependence, while the low energy part of B/C ratio is used to fix a value for the reacceleration level and define the parameters of the LB component.

The heliospheric modulation is treated using the force-field approximation (Gleeson & Axford 1968). In our previous paper (Moskalenko et al. 2002) we used the best currently available model of the heliospheric modulation, the steady-state drift model. The use of the simpler model in the current paper is justified by the following arguments. First, in the previous paper (Moskalenko et al. 2002) we tried to build a model of particle propagation explaining both CR nuclei and antiproton fluxes equally well. The heliospheric modulation calculation was considered as one of the main possible reasons for the discrepancy between the nuclei and antiproton fluxes. It appears however that the interstellar propagation and/or cross section errors are responsible for the nuclei/antiproton discrepancy, unless the current models of heliospheric modulation are *completely* wrong, which is not very likely. Second, the current paper evaluates a new hypothesis for the origin of CR where the main emphasis is on the local CR component. Use of a sophisticated modulation model containing additional unknown variables will make such evaluation unnecessarily complicated. Third, the parameters of the diffusion coefficient are fixed using the data above few GeV where the modulation is weak.

We consider three different models (Table 1) with parameters fixed using the described procedure. They are: the simplest plain diffusion model (PD), and two reacceleration models, which use different assumed isotopic abundances in the Galactic CR sources and LB sources. Diffusive reacceleration model I (DR I) has the same isotopic abundances in Galactic CR and LB sources. Diffusive reacceleration model II (DR II) is the same as DR I except that the LB isotopic abundances are tuned to match

³GALPROP model including software and data sets is available at <http://www.gamma.mpe-garching.mpg.de/~aws/aws.html>

the low-energy data by ACE and Ulysses, thus increasing the freedom to fit the data. The Galactic CR elemental source abundances (DR II model) are tuned to the abundances measured at high energies where the heliospheric modulation is weak.

The plain diffusion model, without an LB component, has already been discussed in Moskalenko et al. (2002). It is inconsistent with low energy data on secondary/primary ratios, and at high energies matching the B/C ratio would cause an overproduction of antiprotons. We do not see a plausible modification of this model, even including an LB component, which would allow to us simultaneously fit antiprotons and the B/C ratio.

Hence we turn to the models with reacceleration. Fig. 1 (left) illustrates the process of fixing the normalization of the diffusion coefficient using antiprotons. The antiproton flux shown as calculated in the DR I/II models with $\delta = 0.47$ and different normalizations in the diffusion coefficient, $D_0 = 2.6 \times 10^{28}, 3.3 \times 10^{28}, 4.3 \times 10^{28} \text{ cm s}^{-2}$ at $\rho = 3 \text{ GV}$ (for antiprotons this corresponds to kinetic energy $\sim 2 \text{ GeV}$). The injection index γ is taken equal to 2.28, and the Alfvén speed $v_A = 23 \text{ km s}^{-1}$. The antiproton flux at maximum, $\sim 2 \text{ GeV}$, appears to be quite sensitive to the value of the diffusion coefficient and allows us to fix it at $D_0 = (3.3 \pm 0.8) \times 10^{28} \text{ cm s}^{-2}$. (A 1σ deviation in the data translates to approximately $-20\%+25\%$ accuracy in D_0 .) The exact value of δ is not critical since we compare with the antiproton measurements at maximum, $\sim 2 \text{ GeV}$. Inelastically scattered antiprotons, the “tertiary” component, appears to be important at low energies only in the ISM. Fig. 1 (right) shows corresponding calculations of the B/C ratio. A halo height of $z_h = 4 \text{ kpc}$ is used (Strong & Moskalenko 2001; Moskalenko, Mashnik, & Strong 2001a); using values differing by up to a factor 2 (the estimated uncertainty) would not affect the conclusions, the diffusion coefficient would simply scale accordingly, $D_0 \propto z_h$ approximately. In Section 6.2 we re-evaluate the radioactive secondaries for the current model and show that our adopted value of z_h is in good agreement with the data.

The local interstellar (LIS) proton and helium spectra used in our antiproton calculations are the best fits to

the data as described in Moskalenko et al. (2002). The proton spectrum is shown in Fig. 2 together with data. Because of the measurements with large statistics, mostly by BESS (Sanuki et al. 2000) and AMS (Alcaraz et al. 2000), and weak heliospheric modulation above 10 GeV, the error arising from uncertainties in the primary spectra is only $\sim 5\%$. The agreement between BESS and AMS data, currently considered to be the most accurate, is impressive. The data collected by other instruments (IMAX, CAPRICE, LEAP) at approximately the same solar modulation level are lower by 5–10% and have larger error bars. Adopting a smaller LIS proton flux would lead to an even more dramatic discrepancy between the antiproton flux data and the calculation in the “standard” reacceleration model (Moskalenko et al. 2002). In any case, allowing for a $\sim 5 - 10\%$ systematic uncertainty in the proton measurements does not change the conclusions of the present paper because the antiproton data have larger error bars.

We note that as in the case of other nuclei, there should be an LB contribution to proton and He spectra. The Galactic injection spectra of protons and He should thus be significantly flatter below several GeV to match the data points at low energies. This does not influence the antiproton production because (i) the LB does not produce a significant amount of secondaries, and (ii) the antiproton threshold production energy is high, $\sim 10 \text{ GeV}$.

Further tuning can be done using the high energy part of the B/C ratio, which is not influenced by heliospheric modulation and supposedly contains only a Galactic component of CR. Fig. 3 (left) shows a calculation of the B/C ratio for $E_b = 500 \text{ MeV}$ and different energy dependencies of the diffusion coefficient. The plotted curves correspond to values of the power-law index $\delta = 0.42, 0.47, 0.52$, while the injection index was tuned to match the high energy spectral data. Index $\delta \sim 0.47$ is chosen as giving the best match. A pure Kolmogorov spectrum, $\delta = 1/3$, thus seems to be excluded by antiproton spectrum data taken in combination with B/C ratio data.

The B/C ratio as calculated with and without a contribution of the LB component is shown in Fig. 3 (right). The LB component is shown calculated with $E_b = 400, 500, 600 \text{ MeV}$. It is seen, however, that all three provide

TABLE 1
PROPAGATION PARAMETER SETS.

Model	Injection index, γ	Diffusion coefficient ^a		Alfvén speed, ^b v_A/\sqrt{w} , km s ⁻¹	Source abundances
		D_0 , cm ² s ⁻¹	Index, δ		
Plain Diffusion (PD)	2.16	3.10×10^{28}	0.60	—	—
Diffusive Reacceleration I (DR I)	2.28	3.30×10^{28}	0.47	23	LBS=CRS
Diffusive Reacceleration II (DR II)	2.28	3.30×10^{28}	0.47	23	LBS≠CRS

Note. — Adopted halo size $z_h = 4 \text{ kpc}$.

^a $\rho_0 = 3 \text{ GV}$.

^b v_A is the Alfvén speed, and w is defined as the ratio of MHD wave energy density to magnetic field energy density.

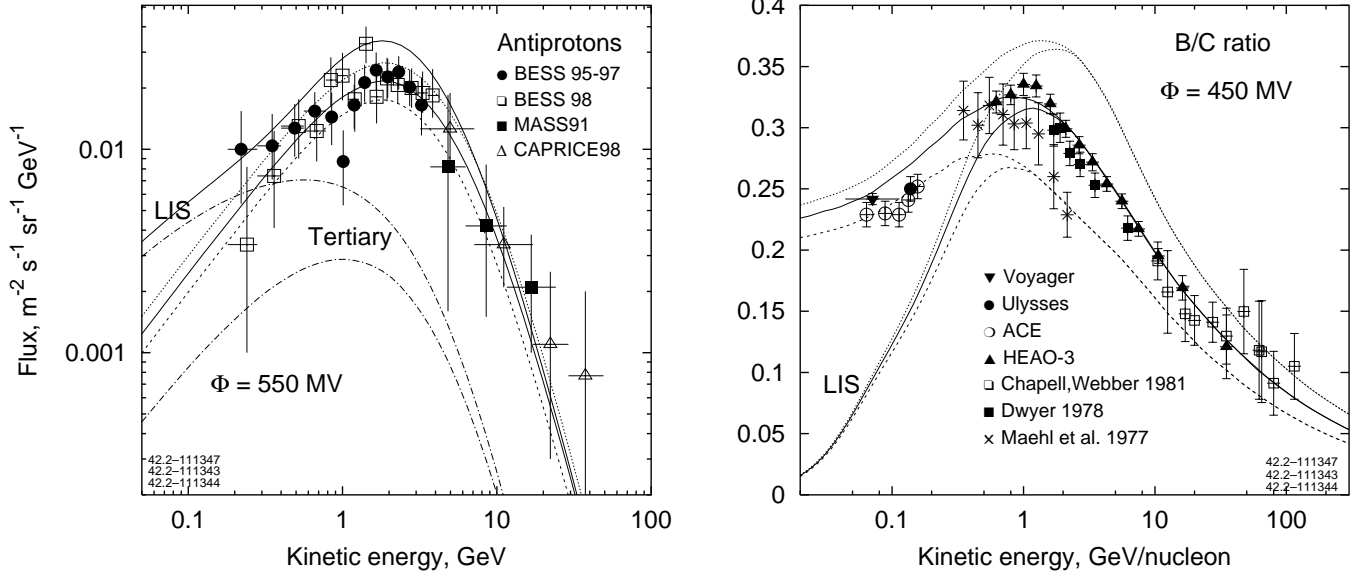


FIG. 1.— *Left*: Antiproton flux calculated in DR I/II models with index $\delta = 0.47$ in the diffusion coefficient and different normalization values, $D_0 \text{ cm s}^{-2}$. Solid curves – $D_0 = 3.3 \times 10^{28}$ at $\rho_0 = 3 \text{ GV}$, upper curve – local interstellar (LIS), lower curve – modulated. Dots – $D_0 = 2.6 \times 10^{28}$, shown modulated only, dashes – $D_0 = 4.3 \times 10^{28}$, shown modulated only. The two lowest curves (dash-dot) marked “tertiary” show separately the LIS spectrum and modulated “tertiary” component for $D_0 = 3.3 \times 10^{28} \text{ cm s}^{-2}$. Modulation was made with $\Phi = 550 \text{ MV}$ (force field). Data: BESS 95-97 (Orito et al. 2000), BESS 98 (Asaoka et al. 2002), MASS91 (Stochaj et al. 2001), CAPRICE98 (Boezio et al. 2001). *Right*: B/C ratio calculated with LB contribution, $E_b = 500 \text{ MeV}$. The lines are coded as on the left panel. Lower curves – LIS, upper – modulated ($\Phi = 450 \text{ MV}$). Data below 200 MeV/nucleon : ACE (Davis et al. 2000), Ulysses (DuVernois, Simpson, & Thayer 1996), Voyager (Lukasiak, McDonald, & Webber 1999); high energy data: HEAO-3 (Engelmann et al. 1990), for other references see Stephens & Streitmatter (1998).

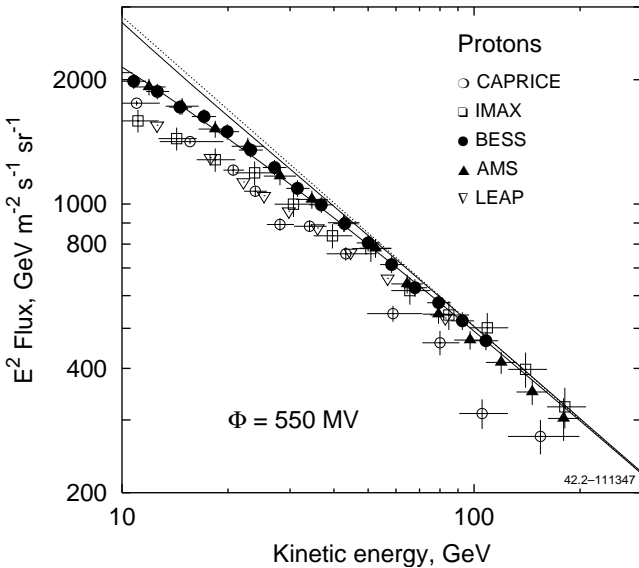


FIG. 2.— The proton spectrum as calculated in models DR I/II compared with the data (upper curve - LIS, lower - modulated to 550 MV). Dotted line shows the LIS spectrum best fitted to the data above 20 GeV (Moskalenko et al. 2002). Data: IMAX (Menn et al. 2000), CAPRICE (Boezio et al. 1999), BESS (Sanuki et al. 2000), AMS (Alcaraz et al. 2000), LEAP (Seo et al. 1991).

good agreement with B/C data. Fig. 4 shows the interstellar and LB carbon spectra in this model. By including the LB component, we have therefore been able to obtain a model simultaneously fitting p , He, \bar{p} and B/C data. It now remains to apply this model to the full range of CR isotopes.

4.1. Calculation uncertainties

We do not discuss here possible calculation *errors*. Derivation of such errors is a *very* complicated matter given the many uncertainties in the input, such as the cross sections, gas distribution in the Galaxy, systematic errors in the CR measurements, heliospheric modulation, atmospheric corrections etc. Some possible errors and their effects have been discussed in Moskalenko et al. (2002). Here we qualitatively mention what we think may affect our conclusions and what may not.

Possible errors in the cross section of the abundant CR nuclei seem to be less important as they can be compensated by relatively small corresponding adjustments in the primary abundances. They however may be more important in case of less abundant “secondary” nuclei. The cross section errors are extensively discussed throughout this paper.

Errors in the Galactic gas distribution are not so important in the case of stable and long-lived nuclei. Such errors are compensated simultaneously for all species by the corresponding adjustment of the propagation parameters (diffusion coefficient).

Heliospheric modulation may introduce some error, but it will be similar for all CR nuclei (or their ratios) because the critical parameter here is the charge-to-mass ratio, approximately $1/2$ for all nuclei except (anti-)protons.

Systematic measurement errors are difficult to account for, but their effect can be reduced by careful choice of the data to rely on. This is what we try to do in the present paper.

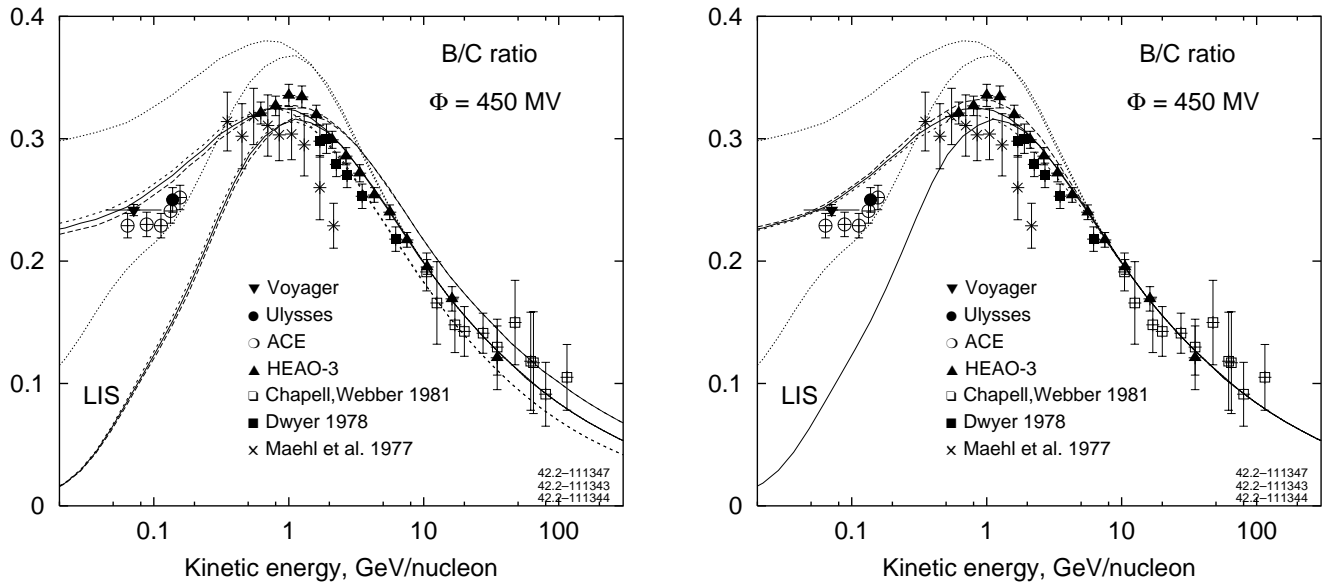


FIG. 3.— *Left*: B/C ratio calculated without (dots) and with (solid, dashes) LB contribution (DR I/II models), $E_b = 500$ MeV/nucleon, with different energy dependence in the diffusion coefficient, $\delta = 0.52$ (short dashes), 0.47 (solid), 0.42 (dashes). Lower curves – interstellar (LIS), upper – modulated ($\Phi = 450$ MV). Data as in Fig. 1 (right). *Right*: B/C ratio calculated without LB contribution (dotted), and with $E_b = 400$ (long dash), 500 (solid), 600 MeV (short dash). Lower curves LIS, upper modulated ($\Phi = 450$ MV). Data as in Fig. 1 (right).

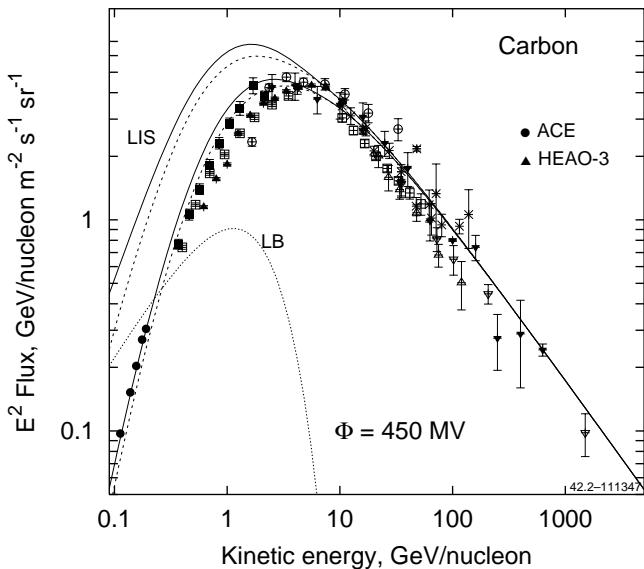


FIG. 4.— Spectrum of carbon calculated with (solid line, model DR II) and without (dashes) LB contribution. Upper curves - LIS, lower curves modulated using force field approximation ($\Phi = 450$ MV). Local Bubble (LB) interstellar spectrum is shown by dots. Data as in Fig. 10.

Such effect as the atmospheric correction to the observed antiproton flux is very important and may affect our results. We discuss it in more details in Sect. 8.

5. APPLICATION TO NUCLEI UP TO NI

The DR I model gives an approximate fit to all elements (Fig. 5). The source elemental abundances are tuned (at a nominal reference energy of 100 GeV), by a least squares procedure, to the abundances measured by HEAO-3 (En-

gelmann et al. 1990) at 7.5, 10.6, 16.2 GeV/nucleon combined with ACE 200 MeV/nucleon data assuming modulation potential $\Phi = 400$ MV. At the chosen HEAO-3 energies the heliospheric modulation is weak (for the epoch 1980 we adopt $\Phi = 800$ MV), and it is in the middle of the logarithmic interval 0.6–35 GeV/nucleon covered by the HEAO-3 measurements; thus the systematic and statistical errors are minimal. To the statistical errors of the ACE data, we added 5% systematic error, which is a minimal conservative estimate of the uncertainties in the measurements and modulation potential.

Fig. 5 shows the quality of the fit. Fig. 5a shows the deviation of the calculated abundances from measurements at a given energy expressed in standard deviations. Fig. 5b shows the average deviation $\langle \Sigma \rangle = \frac{1}{n} \sum_{i=1}^n \frac{A_i^t - A_i^m}{\sigma_i}$, where A_i^t , A_i^m are the calculated and measured abundances for the given energy, and σ_i is the standard deviation. Fig. 5c shows the relative deviation of the calculated abundances from measurements at a given energy.

The DR I fit is systematically low⁴ at low energies (ACE) by as much as 15–30% for elements $Z = 11, 13, 19–25$. It disagrees with high energy abundance of iron by $\sim 20\%$, and by more than 50% for ^{27}Co , and ^{28}Ni . Meanwhile the high energy data taken separately are consistent within 5–10% (Fig. 5c). Because of this low energy discrepancy we consider further only the model DR II, where we allow Galactic CR and LB abundances to be different. In this model, the low energy data are used to determine the LB source abundances. DR II model provides the best fit to all data at the cost of extra free parameters.

In the DR II model, the Galactic CR source elemental abundances are tuned (at a nominal reference energy of 100 GeV), by a least squares procedure, to the abundances

⁴This may be due to the errors in the production cross sections employed in the calculations.

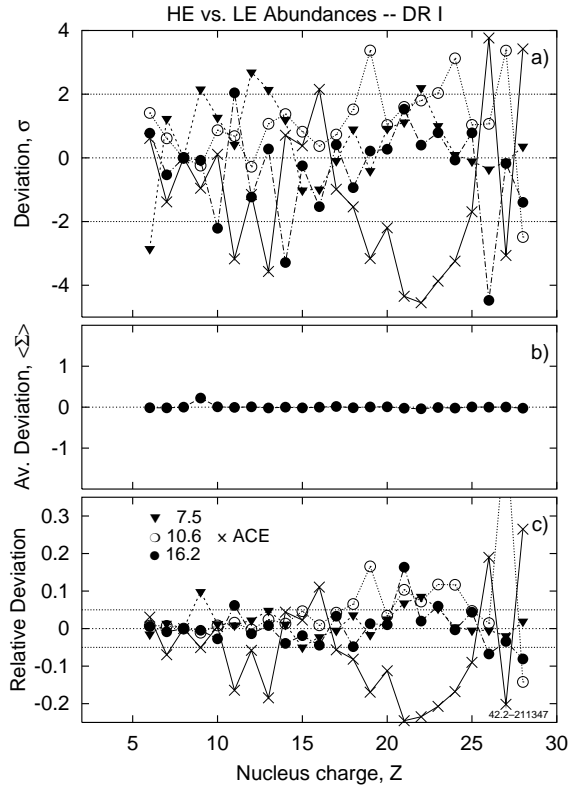


FIG. 5.— Deviation of propagated abundances (model DR I) from measured by HEAO-3 at 7.5, 10.6, 16.2 GeV/nucleon (Engelmann et al. 1990) and ACE at 200 MeV/nucleon (Wiedenbeck et al. 2001) taken together. (a) separately for each energy in σ 's, (b) averaged for four energies in σ 's, and (c) relative.

measured by HEAO-3 (Engelmann et al. 1990) at 5.6, 7.5, 10.6, 16.2 GeV/nucleon (Fig. 6). Fig. 7 shows calculated propagated abundances vs. HEAO-3 data at one particular energy 7.5 GeV/nucleon. Relative isotopic abundances at the source are taken equal to solar system abundances (Anders & Grevesse 1989). The key point in the fitting procedure is to obtain the correct abundance of boron.

Fig. 6 shows the quality of the fit to high energy data, where Figs. 6a,b,c show the deviation of the calculated abundances from measurements at a particular energy expressed in standard deviations, an average deviation, and the relative deviation of the calculated abundances from measurements at a given energy, respectively. The deviations from the data at any particular energy are almost all within $\sim 5\%$. The calculated abundance of ${}^4\text{Be}$ appears to be $\sim 7\%$ below the HEAO-3 data. It is, however, the lightest nucleus measured by the apparatus, and its measurements thus may be affected by systematic errors. Some disagreement in calculated and measured abundances of ${}^9\text{F}$ and ${}^{23}\text{V}$ as seen in Fig. 6b is caused by overproduction at only one energy point, 7.5 GeV/nucleon in case of ${}^9\text{F}$ and 10.6 GeV/nucleon in case of ${}^{23}\text{V}$, while at other energies calculations agree well with data. 10% overproduction of ${}^{24}\text{Cr}$ is seen only at one energy 10.6 GeV/nucleon. Compared to the calculations, measurements of ${}^{19}\text{K}$ and ${}^{27}\text{Co}$ are particularly scattered; ${}^{27}\text{Co}$ is the least abundant element for $Z < 29$ and its abundance in CR is measured with

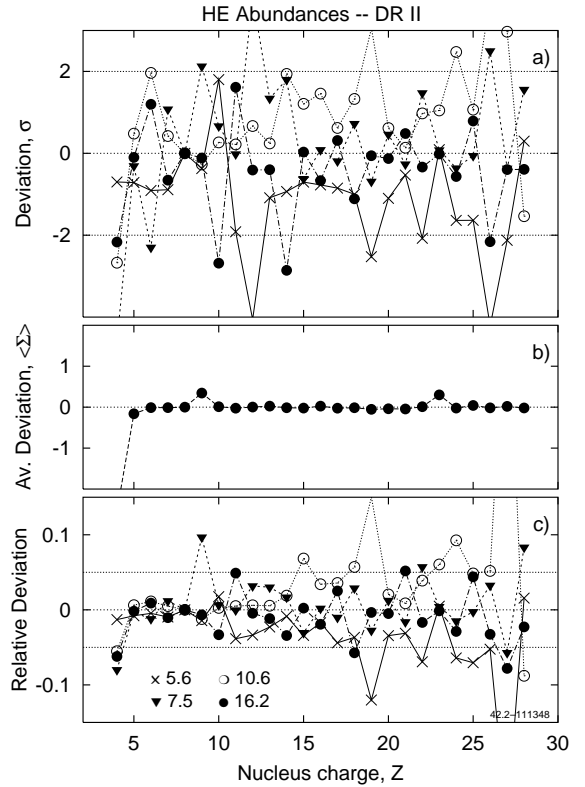


FIG. 6.— Deviation of propagated abundances (model DR II) from measured at 4.3, 5.6, 7.5, 10.6, 16.2 GeV/nucleon (HEAO-3, Engelmann et al. 1990) given (a) separately for each energy in σ 's, (b) averaged for all five energies in σ 's, and (c) relative.

large error bars. ${}^{28}\text{Ni}$ is at the end of the nucleus charge interval measured by HEAO-3 and probably its measurement is also affected by the systematic errors. In general, the deviations in measurements are larger for the least abundant nuclei, which is not surprising.

The LB elemental abundances are tuned simultaneously with spectra using the low energy part of the B/C ratio and isotopic abundances at 200 MeV/nucleon from ACE (Wiedenbeck et al. 2001) and at 185 MeV/nucleon from Ulysses (DuVernois & Thayer 1996). For many elements ACE and Ulysses abundances differ by 10% (Fig. 8c). For this reason, to the statistical errors shown we added 5% systematic error. In the same way as for the high energy data, Fig. 8 shows the quality of the fit to low energy data by ACE and Ulysses.

The fitting procedure is also influenced by the adopted value of the modulation potential. We found that applying the following pairs of modulation potentials yields almost the same LB elemental abundances: 400 MV for ACE and 700 MV for Ulysses, 450 MV – ACE and 600 MV – Ulysses, and 500 MV – ACE and 500 MV – Ulysses. Other combinations of modulation potentials make the quality of the fit worse. The data are shown to deviate from calculations in both directions, which mean that we are unlikely to introduce essential systematic error by assuming a wrong value of the modulation potential.

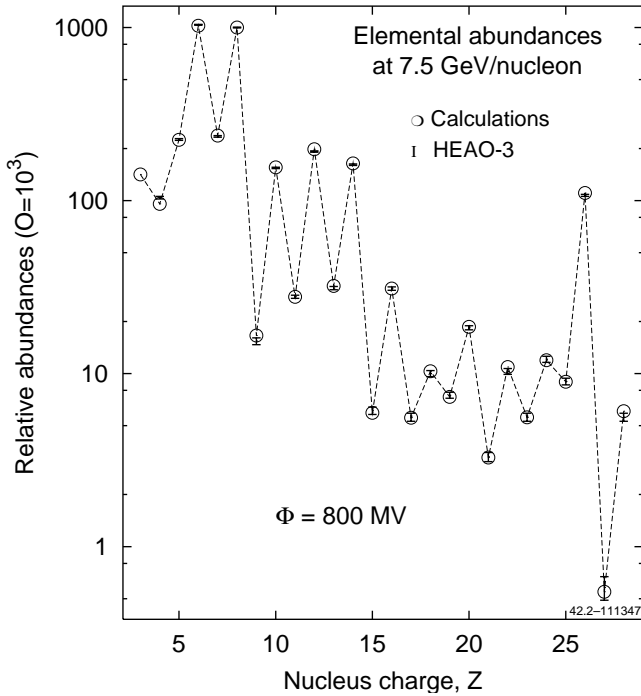


FIG. 7.— Calculated propagated elemental abundances at 7.5 GeV/nucleon (model DR II). Modulation - force field, $\Phi = 800$ MV. Data: HEAO-3 (Engelmann et al. 1990).

6. ABUNDANCES IN COSMIC RAYS AND COSMIC RAY SOURCES

6.1. Elemental abundances in cosmic ray sources

The DR II model with an LB component shows good overall agreement with data including secondary to primary ratios, spectra, and abundances. The derived Galactic CR source abundances and LB source abundances are given in Table 2 and plotted in Fig. 9 relative to the solar system abundances. Spectra of boron, carbon, oxy-

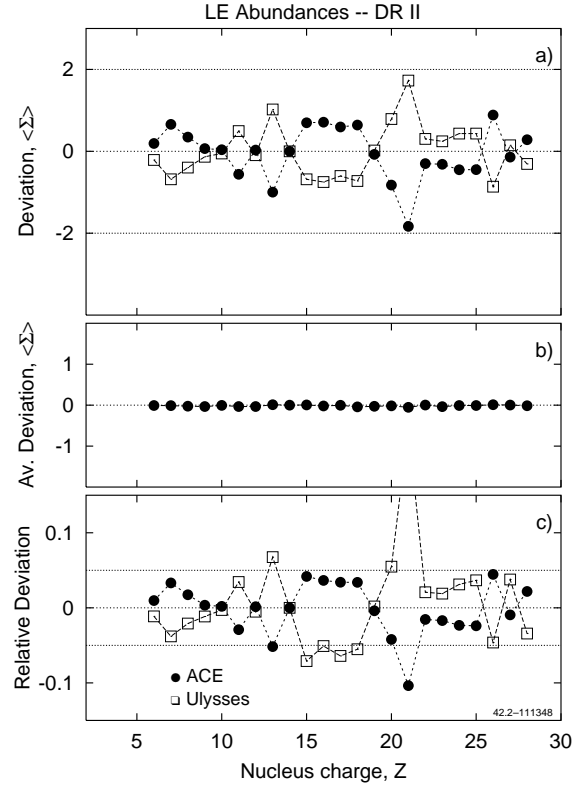


FIG. 8.— Deviation of propagated abundances (model DR II) from measured by ACE (Wiedenbeck et al. 2001) and Ulysses (DuVernois & Thayer 1996) given (a) separately for each energy in σ 's, (b) averaged for both sets of data in σ 's, and (c) relative.

gen, and iron are shown in Fig. 10 for two modulation levels, 450 and 800 MV. In case of carbon, the normalization coefficient in the LB component (eq. [1]) is fixed as $a(6, 12) = 6.35 \times 10^{-4} \text{ cm}^{-2} \text{ s}^{-1} \text{ sr}^{-1}$ for $\eta = 1$. The calculated sub-Fe/Fe ratio is plotted in Fig. 11. Since the elemental abundances are tuned at both high and low energies, it agrees well with data. In the intermediate region at ~ 1 GeV/nucleon, the agreement could be improved by taking E_b smaller than currently assumed 500 MeV (e.g., adopting $E_b = 400$ MeV may raise it by $\sim 10\%$, similar to

TABLE 2
ELEMENTAL ABUNDANCES^a

Z	Solar System	LB Sources	Galactic Sources	Z	Solar System	LB Sources	Galactic Sources
6	9.324	3.850	4.081	18	7.070×10^{-2}	3.283×10^{-2}	1.915×10^{-2}
7	2.344	6.500×10^{-1}	3.022×10^{-1}	19	3.718×10^{-3}	$2.317 \times 10^{-2*}$	6.392×10^{-3}
8	19.04	6.317	5.235	20	6.451×10^{-2}	8.333×10^{-2}	5.887×10^{-2}
9	8.901×10^{-4}	0.	0.	21	4.169×10^{-5}	$1.367 \times 10^{-2*}$	1.730×10^{-4}
10	3.380	6.667×10^{-1}	6.328×10^{-1}	22	2.958×10^{-3}	$5.817 \times 10^{-2*}$	3.166×10^{-3}
11	6.028×10^{-2}	9.767×10^{-2}	3.575×10^{-2}	23	2.817×10^{-4}	$2.433 \times 10^{-2*}$	0.
12	1.070	1.385	1.050	24	1.318×10^{-2}	6.200×10^{-2}	2.481×10^{-2}
13	8.310×10^{-2}	1.583×10^{-1}	7.794×10^{-2}	25	6.901×10^{-3}	1.800×10^{-2}	2.309×10^{-2}
14	1.	1.	1.	26	8.901×10^{-1}	7.767×10^{-1}	9.661×10^{-1}
15	7.944×10^{-3}	5.667×10^{-3}	1.041×10^{-2}	27	2.344×10^{-3}	4.500×10^{-3}	1.773×10^{-3}
16	6.028×10^{-1}	1.000×10^{-1}	1.425×10^{-1}	28	5.014×10^{-2}	3.567×10^{-2}	5.591×10^{-2}
17	8.901×10^{-3}	4.667×10^{-3}	4.047×10^{-3}				

^aNormalized to Si=1.

*Upper limit.

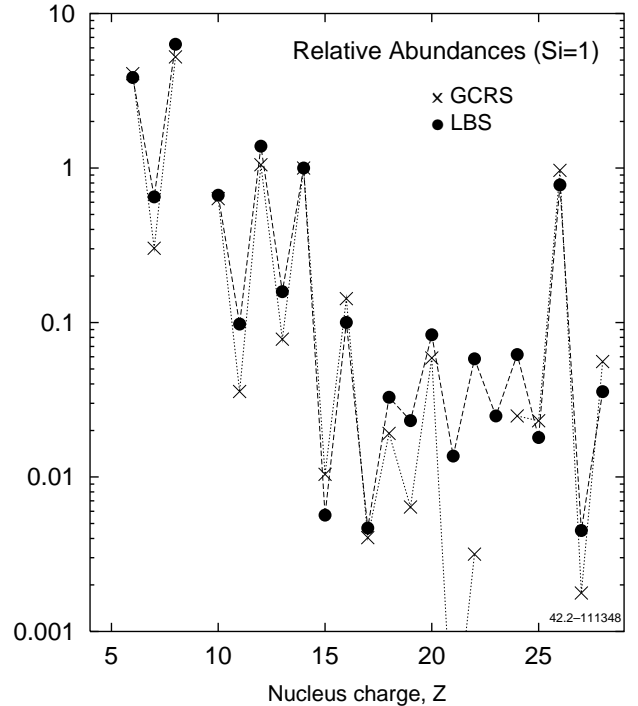
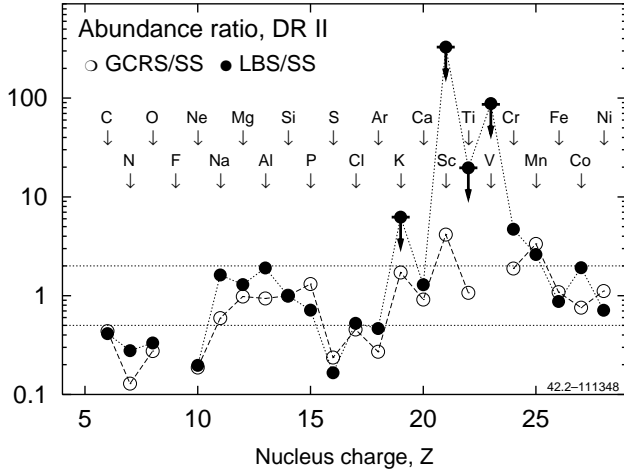


FIG. 9.— *Left*: Derived abundance ratios (model DR II) Galactic-CR-source/Solar-System (GCRS/SS) and LB-source/Solar-System (LBS/SS), normalized to silicon. Relative abundances for K, Sc, Ti, V are shown as upper limits. Solar system abundances from Grevesse & Sauval (1998). The dotted lines plotted at 1/2 and 2. *Right*: Derived Galactic CR source and LB source abundances normalized to silicon.

the change in the B/C ratio, Fig. 3 right).

The important result (Fig. 9) is that CR source and LB source abundances of all major elements (${}_6\text{C}$, ${}_8\text{O}$, ${}_{10}\text{Ne}$, ${}_{12}\text{Mg}$, ${}_{14}\text{Si}$, ${}_{16}\text{S}$, ${}_{18}\text{Ar}$, ${}_{20}\text{Ca}$, ${}_{26}\text{Fe}$, ${}_{28}\text{Ni}$) are in good agreement with each other. Abundances of the Si group, ${}_{20}\text{Ca}$, ${}_{26}\text{Fe}$, ${}_{28}\text{Ni}$ are near the Solar System abundances. Abundances of other elements in Galactic CR and LB sources are mostly consistent with each other, and with solar system abundances, within a factor of 2. Relative to silicon, ${}_6\text{C}$, ${}_7\text{N}$, ${}_8\text{O}$, ${}_{10}\text{Ne}$, ${}_{16}\text{S}$ are underabundant both in CR source and LB. This corresponds to the well-known first-ionization-potential or volatility correlation (see, e.g., Meyer, Drury, & Ellison 1998). Nitrogen in CR sources and LB sources differs by a factor of ~ 3 , which may be connected with production cross section errors affecting propagation of Galactic CR component (see discussion in Appendix A).

Secondary nuclei ${}_{19}\text{K}$, ${}_{21}\text{Sc}$, ${}_{22}\text{Ti}$, ${}_{23}\text{V}$ appear to be overabundant in the LB sources relative to the solar system (shown as upper limits in Fig. 9a), though the derived absolute LB abundances are not large. The derived LB abundance of ${}_{22}\text{Ti}$ does not exceed that of ${}_{24}\text{Cr}$ while the derived abundances of ${}_{21}\text{Sc}$ and ${}_{23}\text{V}$ are not larger than that of ${}_{25}\text{Mn}$ (Fig. 9b). One possible reason for this excess is the uncertainty in the production cross sections, which is especially large for these nuclei. Sometimes there

is no measurement at all; in this case one can use only phenomenological systematics, which are frequently wrong by a factor of two or even more, and/or predictions by Monte Carlo codes. Often, there is only one measurement at ~ 600 MeV/nucleon, which has to be extrapolated in both directions⁵. This allows only a nearly flat Webber-type or Silberberg-Tsao-type extrapolations while the real cross sections usually have large resonances below several hundred MeV, and decrease with energy above a few GeV (see, e.g., Moskalenko, Mashnik, & Strong 2001a). We note that Davis et al. (2000) used semiempirical cross sections based on Webber et al. and also predicted fluxes of sub-Fe elements which are too low.

An estimate of the overall error, which is reflected in the derived LB source abundances, can be obtained by assuming the complete absence of ${}_{19}\text{K}$, ${}_{21}\text{Sc}$, ${}_{22}\text{Ti}$, ${}_{23}\text{V}$ in the LB source (shown by crosses in Fig. 9). In this case the discrepancy between the calculated propagated CR abundances of ${}_{19}\text{K}$, ${}_{21}\text{Sc}$, ${}_{22}\text{Ti}$, ${}_{23}\text{V}$, and those measured is below 20%, and can be removed by allowing the production cross sections to increase at low energies by $\sim 15 - 20\%$, which seems plausible.

Another possibility is errors in flux measurements of the rare CR species. Fig. 12 shows the calculated abundances⁶ tuned at low energies to the ACE and Ulysses data. Ulysses and ACE measurements are not always in

⁵Only the following reactions are well measured (see compilation by Mashnik et al. 1998), on a sample of natural iron consisting mostly of ${}^{56}\text{Fe}$: $p + \text{natFe} \rightarrow {}^{46,47}\text{Sc}$, ${}^{48}\text{V}$, ${}^{48,51}\text{Cr}$; we use our fits to these data. Reactions producing other isotopes of ${}_{21}\text{Sc}$, ${}_{22}\text{Ti}$, ${}_{23}\text{V}$ by ${}^{56}\text{Fe}$, ${}^{55}\text{Mn}$, and ${}^{52}\text{Cr}$ have only one or two measurements. There is no data available on the production of ${}_{21}\text{Sc}$, ${}_{22}\text{Ti}$, ${}_{23}\text{V}$ by ${}^{54}\text{Fe}$, ${}^{53}\text{Mn}$, and ${}_{24}\text{Cr}$ isotopes (except ${}^{52}\text{Cr}$), on production of ${}_{21}\text{Sc}$, ${}_{22}\text{Ti}$, by ${}^{49}\text{V}$, and on production of ${}_{21}\text{Sc}$ by ${}_{22}\text{Ti}$. These poorly known cross sections contribute to errors on the production of sub-Fe elements at low energies.

⁶Calculated Li abundance in the plot shows only secondary lithium produced in CR.

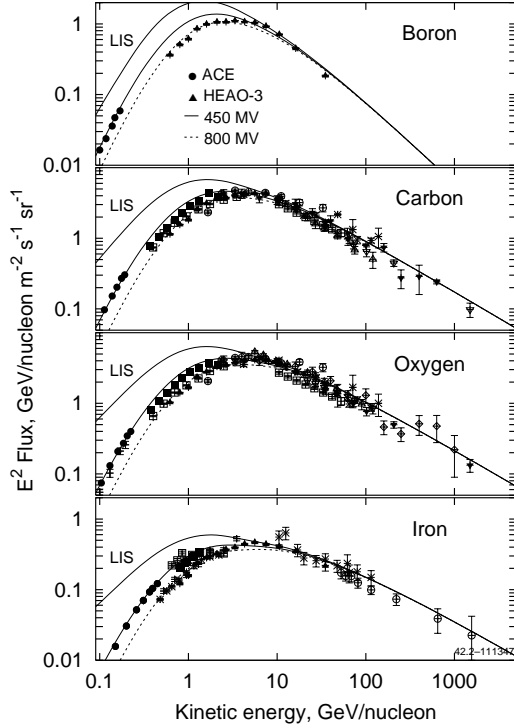


FIG. 10.— Spectra of boron, carbon, oxygen, and iron (from top to bottom) calculated with LB contribution (model DR II). Upper curves - LIS, lower curves - modulated using force field approximation ($\Phi = 450$ MV - solid curves, $\Phi = 800$ MV - dashes). Data: ACE (Davis et al. 2000, 2001), HEAO-3 (Engelmann et al. 1990), for other references see Stephens & Streitmatter (1998) (symbols are changed).

agreement. Note that even for such an abundant nucleus as iron, which is the main contributor to the sub-Fe group, the discrepancy exceeds 10%, while the disagreement in abundance of $_{21}\text{Sc}$ is $\sim 30\%$.

The derived source overabundance of sub-Fe elements in the LB could also in principle arise from composition differences between the ISM in the LB and solar or Galactic average ISM. This is suggested by the fact that the relative abundances of secondary elements in the LB sources are systematically larger than in the Galactic CR sources (Fig. 9). However, the factors required in case of, e.g., $_{22}\text{Ti}$ ($\text{Ti}/\text{Fe} \sim 5\%$ compared to solar or SN 0.1%) appear much larger than could reasonably be expected even for unusual SN types. A similar effect may be caused by a specific correlation between source and gas density distributions (Ptuskin & Soutoul 1990).

6.2. Isotopic distributions in cosmic rays

Be and B isotopes are assumed all secondary, thus there is no possibility to tune them. The DR II model calculation shows perfect agreement with the data on relative isotopic abundances of Be and B (Fig. 13). This is in contrast with a “standard” reacceleration model, where we obtained a 15% discrepancy with relative abundances of ^7Be and ^9Be isotopes (Strong & Moskalenko 2001).

Abundances of stable isotopes of other elements are not very conclusive because they are present in the sources,

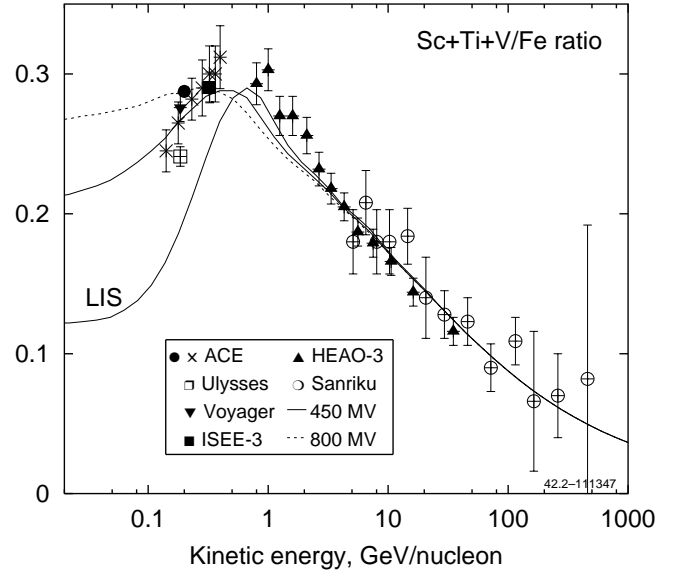


FIG. 11.— Sub-Fe/Fe ratio calculated with LB contribution (model DR II), and with $E_b = 500$ MeV/nucleon. Lower curve - LIS, upper curves - modulated (force field, $\Phi = 450$ and 800 MV). Data: ACE (Wiedenbeck et al. 2001; Davis et al. 2000), Ulysses (DuVernois & Thayer 1996), Voyager (Lukasiak, McDonald, & Webber 1997), ISEE-3 (Leske 1993), HEAO-3 (Engelmann et al. 1990), Sanriku (Hareyama et al. 1999).

but O and Si isotopic distributions still agree very well with data (Webber et al. 1996; Webber, Lukasiak, & McDonald 1997; DuVernois et al. 1996; Hesse et al. 1996; Wiedenbeck et al. 2001) assuming only ^{16}O and ^{28}Si isotopes are present in the LB component. C and N isotopic distributions do not agree too well (Fig. 13), but this may point to a problem with cross sections. The calculated ratio $^{13}\text{C}/^{12}\text{C} \sim 0.11$ at 120 MeV/nucleon ($\Phi = 500$ MV) in the model with LB contribution is still a factor ~ 1.5 too large compared to the measured value, 0.0629 ± 0.0033 (Voyager 50–130 MeV/nucleon, Webber et al. 1996) and 0.078 ± 0.011 (Ulysses 100–200 MeV/nucleon, DuVernois et al. 1996), which may be connected in part with overproduction of ^{13}C by ^{15}N . (A discussion of the cross-section uncertainties for C and N isotopes is given in Appendix A.) If we replace the cumulative cross section $^{15}\text{N}+p \rightarrow ^{13}\text{C}$ with cross section $^{14}\text{N}+p \rightarrow ^{13}\text{C}$, the calculated ratio $^{13}\text{C}/^{12}\text{C}$ will be lowered by 10% as estimated (see Appendix A and Fig. A15). Assuming the absence of the isotope ^{13}C in the Galactic CR sources gives another 10% reduction. Altogether these corrections yield $^{13}\text{C}/^{12}\text{C} \sim 0.09$, close to the data.

Fig. 14 shows calculated $^{10}\text{Be}/^9\text{Be}$, $^{26}\text{Al}/^{27}\text{Al}$, $^{36}\text{Cl}/\text{Cl}$, $^{54}\text{Mn}/\text{Mn}$ ratios, usually used as “radioactive clocks” in CR, for a halo size $z_h = 4$ kpc vs. data. In case of Be, Al, Cl, the agreement with the most accurate low energy data by ACE is very good and all the ratios are consistent with

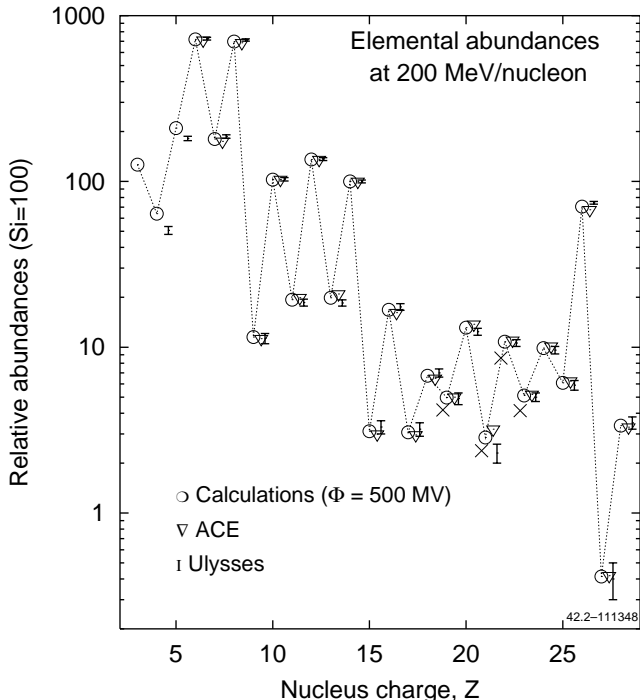


FIG. 12.— Propagated elemental abundances at 200 MeV/nucleon with LB contribution (model DR II). Crosses show the calculated abundances assuming no K, Sc, Ti, V in the LB source. Data: ACE (Wiedenbeck et al. 2001), Ulysses (DuVernois & Thayer 1996).

each other indicating that $z_h = 4$ kpc is a good estimate. Higher energy data by ISOMAX (Be) are also consistent with calculations considering the large error bars.

The $^{54}\text{Mn}/\text{Mn}$ ratio indicates a somewhat smaller halo, but this may be related to uncertainty in its half-life and/or production cross section. The half-life of ^{54}Mn against β^- decay is the most uncertain among the four radioactive isotopes – it is only one which is not measured directly. It is derived indirectly based on β^+ decay branch half-life, which yields an estimate $t_{1/2}(\beta^-) = 6.3 \pm 1.3[\text{stat}] \pm 1.1[\text{theor}] \times 10^5$ yr (Wuosmaa et al. 1998). In case only the half-life is wrong, to get the $^{54}\text{Mn}/\text{Mn}$ ratio consistent with lighter element ratios and with ACE data (for $z_h = 4$ kpc) requires $t_{1/2}(\beta^-) \sim 2$ Myr (Fig. 14). Another estimate of ^{54}Mn partial half-life based on CR propagation calculations gives $\sim 1 - 2$ Myr (DuVernois 1997). Apart from the half-life, a possible source of errors can be production cross sections of Mn isotopes. The fact that the propagated isotopic abundance of ^{53}Mn , $^{53}\text{Mn}/\text{Mn} = 0.50$, is correct (^{53}Mn is a K-capture isotope that is absent in the ISM) indicates that some important production channels of $^{54,55}\text{Mn}$ may be not calculated correctly. (For instance, in case of stable ^{55}Mn , we have a freedom to choose its abundance in the LB component at low energies, which may compensate for underproduction of this isotope in CR. Meanwhile, this LB ^{55}Mn does not produce any ^{54}Mn .) Only the reaction $^{nat}\text{Fe}+p \rightarrow ^{54}\text{Mn}$ on a natural sample of Fe has been measured well enough (see compilation by Mashnik et al. 1998). The cross section

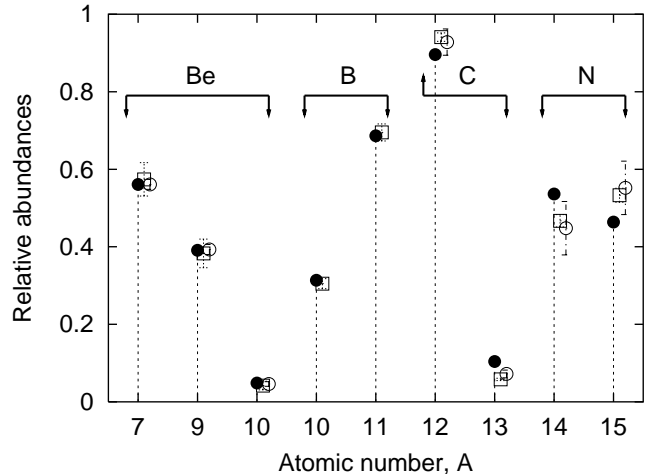


FIG. 13.— Be, B, C, and N isotope distribution as calculated in DR II model (solid circles) at $\sim 70 - 150$ MeV/nucleon and a modulation potential $\Phi = 450 - 500$ MV compare to the data. Data: Be: Ulysses (Connell 1998), Voyager (Lukasiak et al. 1999), B: Voyager (Lukasiak et al. 1999), C,N: Voyager (Webber et al. 1996), Ulysses (DuVernois et al. 1996).

$^{55}\text{Mn}+p \rightarrow ^{54}\text{Mn}$ has only one point measured by Webber et al. (1998b), besides, it seems too low compared to similar neutron knock out reactions on isotopes of Fe and Cr. Reactions $^{55}\text{Fe}+p \rightarrow ^{54}\text{Mn}$, $^{57}\text{Fe}+p \rightarrow ^{54}\text{Mn}$ are not measured at all. Similarly, only one ^{55}Mn major production cross section $^{56}\text{Fe}+p \rightarrow ^{55}\text{Mn}$ has even one point measured.

7. DISCUSSION

The proton spectrum at low energies still remains uncertain. The only secondaries produced below the antiproton production threshold are positrons and γ -rays. However, the positron spectrum *alone* cannot provide conclusive information on the proton spectrum on a large scale because (i) the large energy losses of positrons mean that the positron spectrum by its nature is local (ii) and there are possibly sources of primary positrons such as pulsars. Diffuse γ -rays can provide a tool to test the spectrum of protons in distant regions, but the *a priori* unknown contribution of electrons via inverse Compton and bremsstrahlung complicates the picture. A test of the He spectrum at energies below ~ 10 GeV/nucleon can be made using the CR deuteron and ^3He measurements similar to what was done in this paper for heavier nuclei. We plan to address this issue in future work.

We should mention that there is another possibility to get the correct antiproton flux in reacceleration models, which is to introduce an additional proton component at energies up to approximately 20 GeV. The latter energy is above the antiproton production threshold and effectively produces antiprotons at ~ 2 GeV and below. The intensity and spectral shape of this component could be derived by combining restrictions from antiprotons and diffuse γ -rays. Interestingly this kind of spectrum was used in our HEMN model (hard electrons and modified nucleons, Strong, Moskalenko, & Reimer 2000) to match the spectrum of diffuse γ -rays as observed by EGRET (Hunter et al. 1997). The

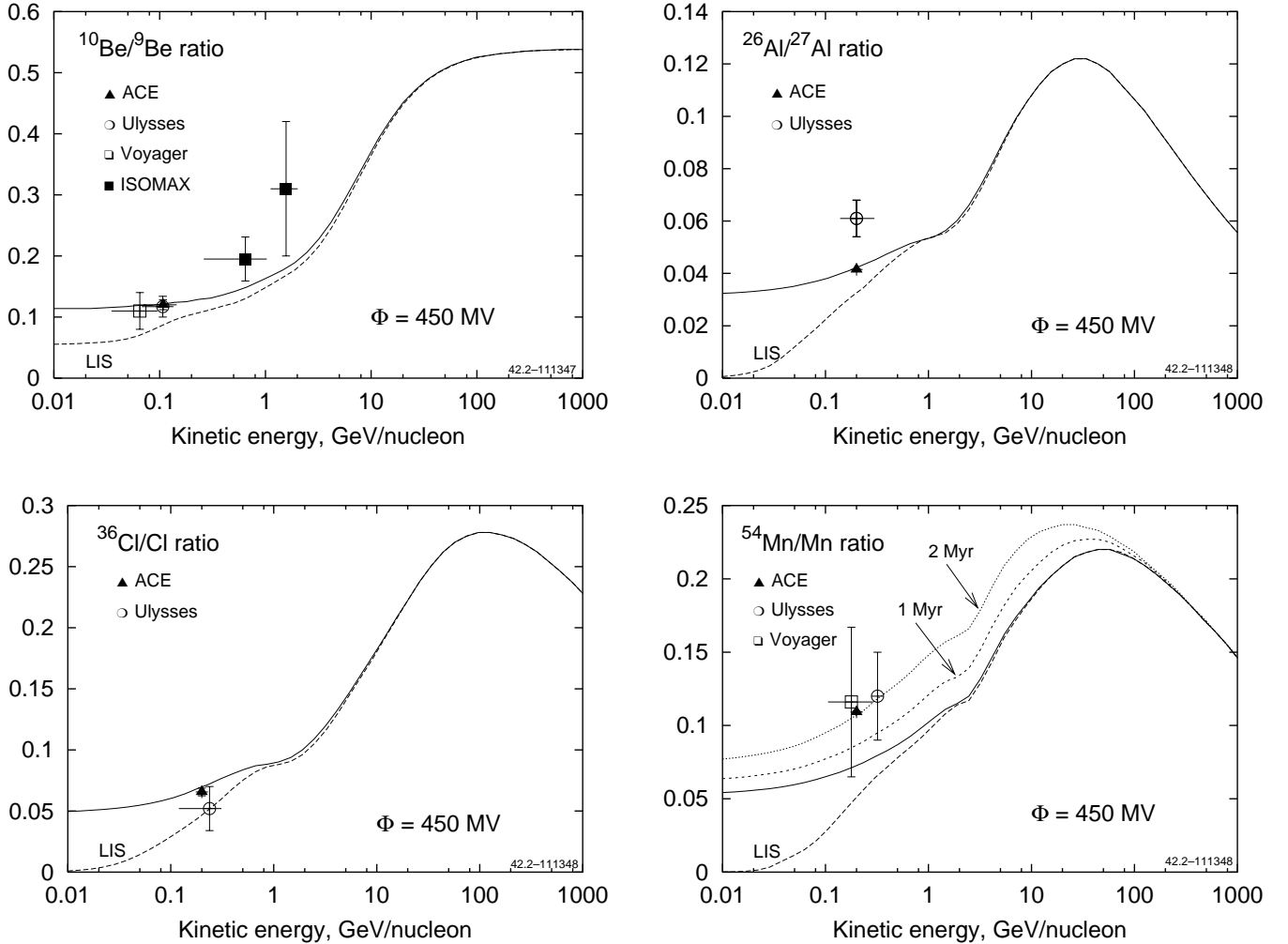


FIG. 14.— “Radioactive clocks” isotopic ratios in CR, as calculated in DR II model for $z_h = 4$ kpc. Dashed curve – interstellar (LIS), solid curve – modulated ($\Phi = 450$ MV). Mn plot shows also the ratio calculated for two half-lives, $t_{1/2} = 1$ Myr and 2 Myr, that are different from the adopted $t_{1/2} = 0.63$ Myr. Be data: Ulysses (Connell 1998), Voyager (Lukasiak et al. 1999), ACE (Binns et al. 1999), ISOMAX (Hams et al. 2001; de Nolfo et al. 2001); Al data: Ulysses (Simpson & Connell 1998), ACE (Wiedenbeck et al. 2001); Cl data: Ulysses (Connell, Duvernois, & Simpson 1998), ACE (Wiedenbeck et al. 2001); Mn data: Ulysses (Duvernois 1997), Voyager (Lukasiak et al. 1997), ACE (Wiedenbeck et al. 2001).

advantage of this approach is that the diffuse γ -rays which we observe carry information on the large-scale Galactic spectrum of CR (producing antiprotons) while particles we measure may reflect only the local region.

One more (non-standard) interpretation is that the solar modulation is weaker than assumed, and this would eliminate the need for a LB component. (A cornerstone of the current theories of heliospheric modulation is the local interstellar spectrum, which is not known but taken *a priori*.) With a modulation potential as small as ~ 200 MV one can obtain a consistent reacceleration model combining B/C, antiprotons, and other species simultaneously. To get an agreement with nucleon spectral data, the injection spectra in such a model should be flatter at low energies than the usually adopted power-law in rigidity.

Recently there has appeared some indication that the atmospheric contribution to the antiproton flux measured in the upper atmosphere is underestimated. Monte Carlo simulations of the hadron cascade development in the up-

per atmosphere have shown that the antiproton flux induced by pA -reactions on air nuclei is larger, *at least*, by $\sim 30\%$ (Huang, Derome, & Buénerd 2001) compared to often employed calculations with analytical production cross sections. This means that the flux of antiprotons in CR in reality may be *lower* at the top of the atmosphere by at least 25-30%. If the latter is true, the reacceleration model (even without LB) could still be the best one to describe propagation of nucleon species in the Galaxy. The inclusion of all known effects such as, e.g., sub-threshold antiproton production on the abundant atmospheric N and O, may be important for evaluation of the correct atmospheric background.

We note that Donato et al. (2001) claim to have obtained agreement with antiproton measurements in a reacceleration plus convection model using the parameters derived from B/C and sub-Fe/Fe ratios (Maurin et al. 2001). Apart from having one more free parameter (convection *plus* reacceleration), they in fact fitted B/C and sub-Fe/Fe

ratios only at high energies (since in their fitting procedure the high energy data overweights few low energy points). Their calculated ratios at low energies are higher than the Voyager and ACE data by approximately 20% or about 6σ (see their Figs. 3, 4 in Maurin et al. 2001). This is, however, where most of the problem lies. Besides, in their nuclear reaction treatment, they use the semiempirical cross sections by Webber et al., which are not particularly accurate at low energies while reacceleration models are sensitive to low energy behaviour of the cross sections.

8. CONCLUSION

In a previous paper we have shown that new more accurate measurements of the CR antiproton flux pose a challenge to existing CR propagation models. In particular, the antiproton flux and B/C ratio appear to be inconsistent with measurements when computed in standard diffusion/reacceleration models. In this paper we have demonstrated that this discrepancy can be resolved if some part of the CR that we measure near the earth consists of a “fresh” component accelerated in the LB. The independent evidence for SN activity in the solar vicinity in the last few Myr supports this idea.

Combining the measurements of the antiproton flux and B/C ratio to fix the diffusion coefficient, we have been able to construct a model consistent with measurements of important nuclei ratios in CR and derive elemental abundances in the LB. Calculated isotopic abundance distributions of Be and B are in perfect agreement with CR data. The abundances of three radioactive isotopes in CR, which are often used as “radioactive clocks” to determine the Galactic halo size, ^{10}Be , ^{26}Al , ^{36}Cl are all consistent and indicate a halo size $z_h \sim 4$ kpc based on the most accurate data by ACE spacecraft. ^{54}Mn indicated a smaller halo, but this may be related to its half-life uncertainty

and/or cross section errors. The derived fraction of LB component in CR is small compared to Galactic CR and has a steep spectrum with a cutoff above several hundred MeV/nucleon. Other experimental data (except maybe the overabundance of Sc, Ti, V) do not contradict this hypothesis. The derived source overabundance of sub-Fe elements in the LB may be caused by trivial uncertainties in the production cross sections, or could in principle arise from composition and/or evolution differences between the ISM in the LB and solar or Galactic average ISM. (LB may have evolved during the sun’s lifetime of 4.5 Gyr.) This is suggested by the fact that the derived relative abundances of secondary elements in the LB sources are systematically larger than in the Galactic CR sources (see, e.g., derivation of interstellar $^{12}\text{C}/^{13}\text{C}$ ratio, Savage et al. 2002).

The production cross sections if measured accurately would help to distinguish between the different hypotheses; as of now, many important channels are not known accurately enough. Such cross section errors lead to errors in important isotopic ratios, which, in turn, are translated into errors in propagation parameters. In our treatment of Be and B production cross sections, as well as some isotopes of other elements, we use all available data and our own fits to them, which should be more accurate than semiempirical systematics by Webber et al. and Silberberg et al.

The authors are grateful to M. Wiedenbeck for providing the ACE isotopic abundances. I. V. M. is grateful to the Gamma Ray Group of the Max-Planck-Institut für extraterrestrische Physik, where a part of this work has been done, for hospitality. I. V. M. and S. G. M. acknowledge partial support from a NASA Astrophysics Theory Program grant.

APPENDIX

PRODUCTION CROSS SECTIONS OF ISOTOPES OF CARBON AND NITROGEN

The production cross section of the most abundant ^{12}C isotope is one of the most poorly known. All the data available to us on its production by ^{16}O and nitrogen isotopes on protons are summarized in Table A3. The data include also production of ^{12}B , and ^{12}N , which decay to ^{12}C with branching ratio 0.98, and ^{13}O with branching ratio 0.12.

Data on the production of ^{13}C are somewhat more extensive, but some important channels are not measured accurately enough. Most of the data available are summarized in Table A4. The data include also production of ^{13}N , which decays to ^{12}C with branching ratio 1. The production cross section of ^{13}B is very small, fractions of a mb. Fortunately there are data on production of ^{13}N by protons on natural samples of oxygen and nitrogen (see compilation by Mashnik et al. 1998), which contain mostly ^{16}O and ^{14}N isotopes respectively. ^{13}N production cross section data probably include also production of ^{13}O , but the latter cross section must be very small (0.17 mb at 2100 MeV/nucleon).

The production cross section of the most abundant ^{14}N isotope is also poorly known. All the data available to us are summarized in Table A5. The compiled data include also production of ^{14}C , and ^{14}O , which decay to ^{14}N with branching ratio 1.

The main contributor to the production cross section of ^{15}N is ^{16}O (Table A6). The direct and indirect (via ^{15}O) production cross sections are almost equal. The channel $p+^{16}\text{O} \rightarrow ^{15}\text{O}$ is well studied since there is a large amount of data obtained on natural sample of oxygen (see compilation by Mashnik et al. 1998).

The cumulative (sum over all channels) production cross sections of carbon and nitrogen isotopes multiplied by the flux of the corresponding primary isotope in CR at 1 GeV/nucleon are shown in Fig. A15. The main contributor to the production of secondary carbon and nitrogen is ^{16}O , accounting for about 80% in case of nitrogen isotopes. However, in

the case of carbon, disintegration of ^{16}O gives only about 50% with an essential contribution from nitrogen isotopes (and ^{13}C in case of ^{12}C).

The contribution of ^{15}N to the production of ^{13}C is especially large (Table A4). This is based on only one experimental point which seems too large compared to the production cross sections on ^{14}N and ^{16}O . This indicates that the reason for the large fraction of ^{13}C in calculated CR abundances compared to the measurements (see Sections 2 and 6) may be errors in the cross sections.

There are more examples of discrepancies in ^{13}C and ^{14}N production cross sections (Tables A4, A5, shown in bold font). The production cross section of ^{13}C by ^{22}Ne at 580 MeV/nucleon differs significantly from that at 400 MeV/nucleon. The cross section of ^{13}C by ^{26}Mg measured by the same group at 370 and 576 MeV/nucleon differs by a factor of 4 (6.3 mb vs. 25 mb). A similar situation occurs with ^{14}C production by ^{22}Ne at 400, 580, and 894 MeV/nucleon, and by ^{26}Mg at 371 and 576 MeV/nucleon (3.5 mb vs. 9 mb). Fortunately, these latter cross sections do not contribute much to production of ^{13}C and ^{14}N in CR, but these discrepancies indicate the degree of overall uncertainty in the production cross sections.

Cross section errors in production of carbon may lead to errors in the B/C ratio, which, in turn, are translated into errors on the propagation parameters. Because the CR measurements are now rather accurate, the errors in the cross sections may cause many standard deviations when comparing the model calculations with CR data.

It is clear that a more systematic approach to calculated cross sections is required such as using, e.g., evaluated cross sections in future similar work instead of only scarce experimental data or calculations by stand-alone nuclear reaction models or phenomenological systematics. Such evaluated data files (Mashnik et al. 1998) have proved to be useful, e.g., to study the production of radioisotopes for medical and industrial applications using high power accelerators (Van Riper, Mashnik, & Wilson 2001). At present, neither available experimental data nor any of the current models or phenomenological systematics can be used alone to produce a reliable evaluated activation cross section library covering a wide range of target nuclides and incident energies. Instead, such an evaluated library may be created by constructing excitation functions using all available experimental data along with calculations employing some of the most reliable codes in the regions of targets and incident energies where they are most applicable. When there are reliable experimental data, they, rather than model results, should be taken as the highest priority for the evaluation. The development of such evaluated data libraries for astrophysical applications is planned in the near future.

TABLE A3
COLLECTION OF ^{12}C PRODUCTION CROSS SECTION DATA ON PROTONS.

Primary Nucleus	Secondary Nucleus	Energy, MeV/nucleon	Cross section, mbarn	Error, mbarn	Reference
^{14}N	^{12}C	377	56.90	0.05 ^a	1
^{14}N	—	516	52.10	0.05 ^b	2
^{15}N	—	373	30.00	0.05 ^a	1
^{16}O	—	389	33.90	0.05 ^a	1
^{16}O	—	516	33.60	0.05 ^b	2
^{16}O	—	2100	32.30	4.80	3
^{16}O	^{12}B	516	1.10	0.30 ^b	2
^{16}O	—	2100	1.45	0.17	3
^{14}N	^{12}N	516	1.10	0.30 ^b	2
^{16}O	—	516	0.30	0.30 ^b	2
^{16}O	—	2100	0.40	0.07	3

^aRelative error.

^bRelative error is shown as indicated in Webber et al. (1998a).

References. — (1) Webber et al. (1998a); (2) Webber et al. (1990a); (3) Olson et al. (1983).

TABLE A4
COLLECTION OF ^{13}C PRODUCTION CROSS SECTION DATA ON PROTONS.

Primary Nucleus	Secondary Nucleus	Energy, MeV/nucleon	Cross section, mbarn	Error, mbarn	Reference
^{14}N	^{13}C	377	7.60	0.05 ^a	1
^{14}N	—	516	9.60	0.05 ^b	2
^{15}N	—	373	35.30	0.05 ^a	1
^{16}O	—	389	17.40	0.05 ^a	1
^{16}O	—	516	18.00	0.05 ^b	2
^{16}O	—	2100	17.80	1.70	3
^{20}Ne	—	414	15.30	0.05 ^a	1
^{20}Ne	—	534	15.70	0.05 ^b	2
^{22}Ne	—	377	17.80	1.40	4
^{22}Ne	—	401	15.30	0.05 ^a	1
^{22}Ne	—	581	21.90	1.90	4
^{22}Ne	—	894	19.00	1.60	4
^{26}Mg	—	371	6.30	1.20	4
^{26}Mg	—	576	25.00	2.80	4
$^{nat}\text{N}(^{14}\text{N})$	^{13}N		multi-data		5
^{14}N	—	377	7.40	0.10 ^a	1
^{14}N	—	516	7.50	0.10 ^b	2
^{15}N	—	373	4.30	0.30 ^a	1
$^{nat}\text{O}(^{16}\text{O})$	—		multi-data		5
^{16}O	—	389	4.60	0.20 ^a	1
^{16}O	—	516	5.70	0.20 ^b	2
^{16}O	—	2100	4.49	0.46	3
^{20}Ne	—	414	5.10	0.20 ^a	1
^{20}Ne	—	534	4.10	0.20 ^b	2
^{22}Ne	—	377	0.50	0.10	4
^{22}Ne	—	401	1.60	0.20 ^a	1
^{22}Ne	—	581	0.50	0.10	4
^{22}Ne	—	894	0.70	0.20	4
^{24}Mg	—	610	6.00	0.20 ^b	2
^{26}Mg	—	371	0.30	0.10	4
^{26}Mg	—	576	0.10	0.10	4

Note. — Discrepancy in the data is shown in bold.

^aRelative error.

^bRelative error is shown as indicated in Webber et al. (1998a).

References. — (1) Webber et al. (1998a); (2) Webber et al. (1990a); (3) Olson et al. (1983); (4) Chen et al. (1997); (5) a compilation by Mashnik et al. (1998).

TABLE A5
COLLECTION OF ^{14}N PRODUCTION CROSS SECTION DATA ON PROTONS.

Primary Nucleus	Secondary Nucleus	Energy, MeV/nucleon	Cross section, mbarn	Error, mbarn	Reference
^{15}N	^{14}N	373	27.60	0.05 ^a	1
^{16}O	—	389	31.10	0.05 ^a	1
^{16}O	—	516	31.00	0.05 ^b	2
^{16}O	—	2100	31.00	3.30	3
^{20}Ne	—	414	25.80	0.05 ^a	1
^{22}Ne	—	401	11.60	0.10 ^a	1
^{15}N	^{14}C	373	10.30	0.05 ^a	1
^{16}O	—	389	1.70	0.10 ^a	1
^{16}O	—	516	1.70	0.10 ^b	2
^{16}O	—	2100	3.69	0.38	3
^{20}Ne	—	414	2.20	0.10 ^a	1
^{20}Ne	—	534	2.30	0.10 ^b	2
^{22}Ne	—	377	8.10	0.70	4
^{22}Ne	—	401	7.70	0.05 ^a	1
^{22}Ne	—	581	10.20	1.20	4
^{22}Ne	—	894	8.60	0.90	4
^{26}Mg	—	371	3.50	0.70	4
^{26}Mg	—	576	9.00	1.30	4
^{16}O	^{14}O	389	1.30	0.30 ^a	1
^{16}O	—	516	1.20	0.30 ^b	2
^{16}O	—	2100	0.75	0.12	3
^{20}Ne	—	534	1.00	0.30 ^b	2
^{24}Mg	—	610	1.50	0.30 ^b	2

Note. — Discrepancy in the data is shown in bold.

^aRelative error.

^bRelative error is shown as indicated in Webber et al. (1998a).

References. — (1) Webber et al. (1998a); (2) Webber et al. (1990a); (3) Olson et al. (1983); (4) Chen et al. (1997).

TABLE A6
COLLECTION OF ^{15}N PRODUCTION CROSS SECTION DATA ON PROTONS.

Primary Nucleus	Secondary Nucleus	Energy, MeV/nucleon	Cross section, mbarn	Error, mbarn	Reference
^{16}O	^{15}N	389	33.60	0.05 ^a	1
^{16}O	—	516	34.90	0.05 ^b	3
^{16}O	—	2100	34.30	3.30	4
^{20}Ne	—	414	24.00	0.05 ^a	1
^{20}Ne	—	534	27.80	0.05 ^b	3
^{22}Ne	—	377	36.20	2.10	5
^{22}Ne	—	401	32.90	0.05 ^a	1
^{22}Ne	—	581	39.00	2.50	5
^{22}Ne	—	894	33.50	2.10	5
^{24}Mg	—	610	14.00	0.10 ^b	3
^{26}Mg	—	371	19.70	2.10	5
^{26}Mg	—	576	29.90	3.00	5
^{22}Ne	^{15}C	377	0.70	0.20	5
^{22}Ne	—	581	0.80	0.20	5
^{22}Ne	—	894	0.60	0.10	5
^{26}Mg	—	371	0.90	0.30	5
^{26}Mg	—	576	0.40	0.30	5
$^{nat}\text{O}(^{16}\text{O})$	^{15}O		multi-data		6
^{16}O	—	389	30.70	0.05 ^a	1
^{16}O	—	516	30.30	0.05 ^b	3
^{16}O	—	2100	27.30	2.60	4
^{20}Ne	—	414	14.90	0.10 ^a	1
^{20}Ne	—	534	16.20	0.10 ^b	3
^{21}Ne	—	520	7.80	0.30 ^a	2
^{22}Ne	—	377	2.00	0.30	5
^{22}Ne	—	401	1.60	0.20 ^a	1
^{22}Ne	—	581	1.60	0.30	5
^{22}Ne	—	894	2.80	0.40	5
^{22}Na	—	520	10.90	0.30 ^a	2
^{23}Na	—	517	11.10	0.30 ^a	2
^{24}Mg	—	610	8.60	0.10 ^b	3
^{25}Mg	—	514	6.00	0.30 ^a	2
^{26}Mg	—	371	1.10	0.30	5
^{26}Mg	—	576	0.20	0.20	5
^{26}Al	—	508	4.10	0.30 ^a	2
^{27}Al	—	511	7.10	0.20 ^a	2
^{28}Si	—	506	5.60	0.12 ^a	2
^{29}Si	—	508	2.40	0.30 ^a	2

Note. — Discrepancy in the data is shown in bold.

^aRelative error.

^bRelative error is shown as indicated in Webber et al. (1998a).

References. — (1) Webber et al. (1998a); (2) Webber et al. (1998b); (3) Webber et al. (1990a); (4) Olson et al. (1983); (5) Chen et al. (1997); (6) a compilation by Mashnik et al. (1998).

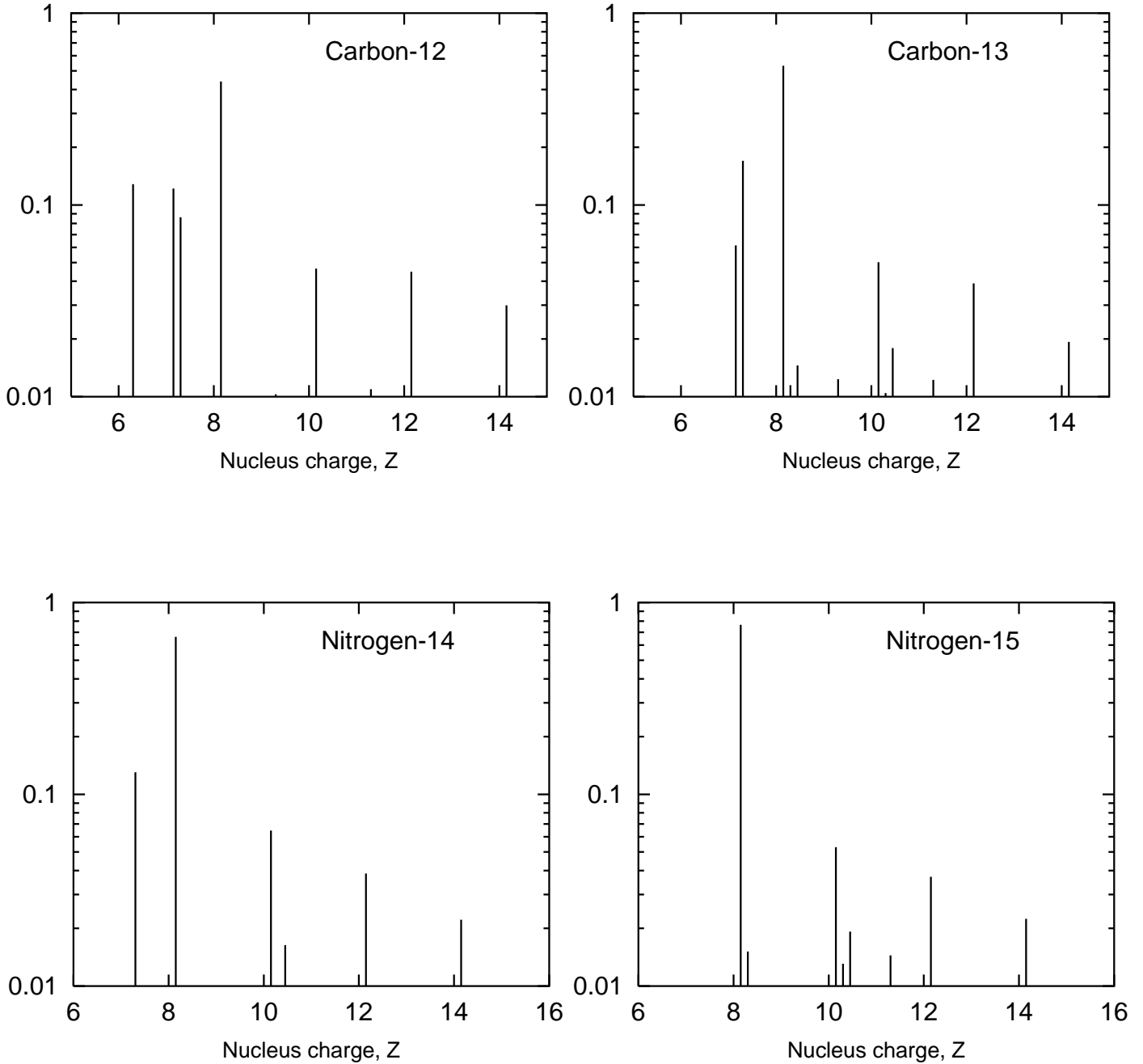


FIG. A15.— Relative contributions of heavier isotopes to production of carbon and nitrogen isotopes are shown. These contributions are determined from cumulative cross sections of carbon and nitrogen isotopes weighted with the flux of corresponding primary isotope in CR at 1 GeV/nucleon. The contributions of isotopes of a given element are indicated by separate lines. The scale gives the fraction of the C and N isotope produced by a given primary isotope.

REFERENCES

- Alibés, A., Labay, J., & Canal, R. 2001, *A&A*, submitted, astro-ph/0107016
- Alcaraz, J., et al. 2000, *Phys. Lett. B*, 490, 27
- Anders, E., & Grevesse, N. 1989, *Geochim. Cosmochim. Acta*, 53, 197
- Asaoka, Y., et al. 2002, *Phys. Rev. Lett.*, 88, 051101
- Benítez, N., Maíz-Apellániz, J., & Canelles, M. 2002, *Phys. Rev. Lett.*, 88, 081101
- Berghöfer, T. W., & Breitschwerdt, D. 2002, *A&A*, 299
- Binns, W. R., et al. 1999, *Proc. 26th Int. Cosmic Ray Conf. (Salt Lake City)*, 3, 21
- Boezio, M., et al. 1999, *ApJ*, 518, 457
- Boezio, M., et al. 2001, *ApJ*, 561, 787
- Bogomolov, E. A., Lubyayana, N. D., Romanov, V. A., & Stepanov, S. V., & Shulakova, M. S. 1979, *Proc. 16th Int. Cosmic Ray Conf. (Kyoto)*, 1, 330
- Bykov, A. M. 2001, *Space Sci. Rev.*, 99, 317
- Bykov, A. M., & Fleishman, G. D. 1992, *MNRAS*, 255, 269
- Chen, C.-X., et al. 1997, *ApJ*, 479, 504
- Connell, J. J. 1998, *ApJ*, 501, L59
- Connell, J. J., Duvernois, M. A., & Simpson, J. A. 1998, *ApJ*, 509, L97
- Davis, A. J., et al. 2000, in *AIP Conf. Proc. 528, Acceleration and Transport of Energetic Particles Observed in the Heliosphere (ACE-2000)*, ed. R. A. Mewaldt et al. (New York: AIP), 421
- Davis, A. J., et al. 2001, *Proc. 27th Int. Cosmic Ray Conf. (Hamburg)*, 3971
- de Nolfo, G. A., et al. 2001, *Proc. 27th Int. Cosmic Ray Conf. (Hamburg)*, 1659
- Donato, F. et al. 2001, *ApJ*, 563, 172
- Duvernois, M. A. 1997, *ApJ*, 481, 241
- Duvernois, M. A., Simpson, J. A., & Thayer, M. R. 1996, *A&A*, 316, 555
- Duvernois, M. A., & Thayer, M. R. 1996, *ApJ*, 465, 982
- Duvernois, M. A., Garcia-Munoz, M., Pyle, K. R., Simpson, J. A., & Thayer, M. R. 1996, *ApJ*, 466, 457
- Engelmann, J. J., et al. 1990, *A&A*, 233, 96
- Gleeson, L. J., & Axford, W. I. 1968, *ApJ*, 154, 1011
- Golden, R. L., Horan, S., Mauger, B. G., Badhwar, G. D., Lacy, J. L., Stephens, S. A., Daniel, R. R., & Zipse, J. E. 1979, *Phys. Rev. Lett.*, 43, 1196
- Grevesse, N., & Sauval, A. J. 1998, *Space Sci. Rev.*, 85, 161
- Hams, T., et al. 2001, *Proc. 27th Int. Cosmic Ray Conf. (Hamburg)*, 1655
- Hareyama, M., et al. 1999, *Proc. 26th Int. Cosmic Ray Conf. (Salt Lake City)*, 3, 105
- Hesse, A., et al. 1996, *A&A*, 314, 785
- Higdon, J. C., Lingenfelter, R. E., & Ramaty, R. 1998, *ApJ*, 509, L33
- Huang, C. Y., Derome, L., & Buénerd, M. 2001, *Proc. 27th Int. Cosmic Ray Conf. (Hamburg)*, 1707
- Hunter, S. D., et al. 1997, *ApJ*, 481, 205
- Jones, F. C., Lukasiak, A., Ptuskin, V., & Webber, W. 2001, *Proc. 27th Int. Cosmic Ray Conf. (Hamburg)*, 1844
- Jones, F. C., Lukasiak, A., Ptuskin, V., & Webber, W. 2001, *ApJ*, 547, 264
- Knies, K., Korschinek, G., Faestermann, T., Wallner, C., Scholten, J., & Hillebrandt, W. 1999, *Phys. Rev. Lett.*, 83, 18
- Leske, R. A. 1993, *ApJ*, 405, 567
- Lukasiak, A., McDonald, F. B., & Webber, W. R. 1997, *ApJ*, 488, 454
- Lukasiak, A., McDonald, F. B., & Webber, W. R. 1999, *Proc. 26th Int. Cosmic Ray Conf. (Salt Lake City)*, 3, 41
- Maiz-Apellániz, J. 2001, *ApJ*, 560, L83
- Mashnik, S. G., Sierk, A. J., Van Riper, K. A., & Wilson, W. B. 1998, *Proc. 4th Workshop on Simulating Accelerator Radiation Environments*, ed. Gabriel, T. A. (Oak Ridge: ORNL), 151 (nucl-th/9812071)
- Maurin, D., Donato, F., Taillet, R., & Salati, P. 2001, *ApJ*, 555, 585
- Menn, W. et al. 2000, *ApJ*, 533, 281
- Meyer, J.-P., Drury, L. O'C., & Ellison, D. C. 1998, *Space Sci. Rev.*, 86, 179
- Mitchell, J. W., et al. 1996, *Phys. Rev. Lett.*, 76, 3057
- Molnar, A., & Simon, M. 2001, *Proc. 27th Int. Cosmic Ray Conf. (Hamburg)*, 1877
- Morfill, G. E., & Freyberg, M. J. 1998, in *Lecture Notes in Physics 506, The Local Bubble and Beyond*, *Proc. IAU Colloquium No. 166*, ed. by D. Breitschwerdt et al. (Berlin: Springer), 177
- Moskalenko, I. V., Mashnik, S. G., & Strong, A. W. 2001a, *Proc. 27th Int. Cosmic Ray Conf. (Hamburg)*, 1836
- Moskalenko, I. V., Strong, A. W., Ormes, J. F., Potgieter, M. S., & Langner, U. W. 2001b, *Proc. 27th Int. Cosmic Ray Conf. (Hamburg)*, 1868
- Moskalenko, I. V., Strong, A. W., Ormes, J. F., & Potgieter, M. S. 2002, *ApJ*, 565, 280
- Olson, D. L., et al. 1983, *Phys. Rev. C*, 28, 1602
- Orito, S., et al. 2000, *Phys. Rev. Lett.*, 84, 1078
- Ptuskin, V. S., & Soutoul, A. 1990, *A&A*, 237, 445
- Van Riper, K. A., Mashnik, S. G., & Wilson, W. B. 2001, *Nucl. Instrum. Meth. A*, 463, 576
- Sanuki, T., et al. 2000, *ApJ*, 545, 1135
- Savage, C., et al. 2002, *ApJ*, 578, 211
- Seo, E. S., et al. 1991, *ApJ*, 378, 763
- Sfeir, D. M., Lallement, R., Crifo, F., & Welsh, B. Y. 1999, *A&A*, 346, 785
- Silberberg, R., Tsao, C. H., & Barghouty, A. F. 1998, *ApJ*, 501, 911
- Simpson, J. A. & Connell, J. J. 1998, *ApJ*, 497, L85
- Sonett, C. P., Morfill, G. E., & Jokipii, J. R. 1987, *Nature*, 330, 458
- Stephens, S. A., & Streitmatter, R. A. 1998, *ApJ*, 505, 266
- Stochaj, S. J., et al. 2001, *ApJ*, in press
- Strong, A. W., & Moskalenko, I. V. 1998, *ApJ*, 509, 212
- Strong, A. W., & Moskalenko, I. V. 2001, *Adv. Space Res.*, 27, 717
- Strong, A. W., Moskalenko, I. V., & Reimer, O. 2000, *ApJ*, 537, 763; Erratum: 2000, *ApJ*, 541, 1109
- Webber, W. R., Kish, J. C., & Schrier, D. A. 1990a, *Phys. Rev. C*, 41, 547
- Webber, W. R., Kish, J. C., & Schrier, D. A. 1990b, *Phys. Rev. C*, 41, 566
- Webber, W. R., Lukasiak, A., McDonald, F. B., & Ferrando, P., 1996, *ApJ*, 457, 435
- Webber, W. R., Lukasiak, A., & McDonald, F. B., 1997, *ApJ*, 476, 766
- Webber, W. R., et al. 1998a, *ApJ*, 508, 949
- Webber, W. R., et al. 1998b, *Phys. Rev. C*, 58, 3539
- Wiedenbeck, M. E., et al. 2001, *Space Sci. Rev.*, 99, 15
- Wuosmaa, A. H., et al. 1998, *Phys. Rev. Lett.*, 80, 2085